X-ray dislocation substructure observations and strengthening mechanisms in α-iron single crystal between room temperature and 123 K

G. Coulon, J. Lecoq, B. Escaig

Classification
Physics Abstracts
9.126

X-RAY DISLOCATION SUBSTRUCTURE OBSERVATIONS AND STRENGTHENING MECHANISMS IN α-IRON SINGLE CRYSTAL BETWEEN ROOM TEMPERATURE AND 123 K

G. COULON, J. LECOQ and B. ESCAIG

Laboratoire de Physique des Défauts de l'Etat Solide (*)
Université des Sciences et Techniques de Lille BP 36, 59650 Villeneuve d'Ascq, France

(*Reçu le 2 octobre 1973*)

Résumé. — La consolidation du fer α monocristallin a été étudiée sur le système $(\bar{1}01)$ [111] entre 296 K et 123 K jusqu'à 20 % de déformation. Les paramètres d'activation thermique ont été mesurés tout le long de la courbe de déformation par relaxation de la contrainte appliquée et par des essais différentiels en fluage, parallèlement on a examiné la sous-structure de dislocations par topographie X de Berg-Barrett. En-dessous de 200 K, la sous-structure de dislocations observée est homogène, le volume d'activation est indépendant de la déformation et les courbes contrainte-cisaillement réduits présentent un taux de durcissement quasiment nul : toute la plasticité est régie par le seul frottement de réseau. Au-dessus de 200 K, la sous-structure de dislocations devient de plus en plus hétérogène au fur et à mesure que la température croît, le volume d'activation décroît avec la déformation et le taux de durcissement n'est plus nul et vaut $10^{-3}\,\mu$: l'activation thermique l'emporte sur le frottement de réseau.

Abstract. — α-Iron single crystals have been investigated in the $(\bar{1}01)$ [111] slip system between 123 and 296 K up to 20 % deformation. Stress relaxation and creep tests have been used to measure activation parameters during tensile straining. Berg-Barrett X-ray reflection topography was used to examine the overall dislocation substructure. Below 200 K the observed dislocation substructure is homogeneous ; the activation volume is independent of strain and the stress-strain curves show an almost zero work-hardening rate : the whole plasticity is controlled solely by the Peierls friction. Above 200 K the dislocation substructure becomes more and more heterogeneous as temperature increases ; the activation volume decreases with strain and the work-hardening rate is around $10^{-3}\,\mu$: thermal activation overcomes the lattice friction.

1. **Introduction.** — The purpose of this paper is to study the low temperature plastic behaviour of α-iron single crystals [18].

The origin of the elastic limit in pure b. c. c. crystals is now well known. Several investigations have revealed that its rapid decrease with increasing temperature stems from a strong intrinsic interaction between screw dislocations and the crystal lattice.

On the contrary the mechanism controlling b. c. c. work-hardening is much less understood.

Thus recent experimental studies of work-hardening in high-purity crystals of molybdenum [1, 2], niobium [3, 4], and iron [5, 6, 7] have shown that the stress-strain curves change from a three-stage hardening shape to a parabolic one with decreasing temperature.

Furthermore the dislocation substructure has been mainly investigated by electron microscopy, after tensile deformation at 293 K. In a few reports the 293 K dislocation substructure has been compared to a lower-temperature one : 158 K for Nb [4], 173 K for α-Fe [7].

But these observations do not describe the overall process and do not allow one to understand how lattice friction influences plasticity.

At lower temperatures the interaction between screw dislocations and the crystal lattice is expected to be large enough to prevent any dislocation rearrangement during the deformation. Thus the whole plasticity might be controlled by lattice friction alone.

In the upper part of the temperature range, however, the decreasing lattice friction should allow primary and conjugated slip systems to interact. Internal stresses due to the resulting tangles should then superimpose upon the Peierls friction and give rise to a

(*) Equipe de Recherche associée au C. N. R. S. n° 374.

different plastic behaviour, the study of which is the purpose of our investigation. The evolution of macroscopic deformation parameters has been examined between room temperature and 123 K, at tensile shear strains up to 0.2. Creep, stress relaxation, and standard tensile tests have been used and correlated with a systematic observation of the dislocation substructure by means of the Berg-Barrett X-ray technique [8]. As compared with electron microscopy, this method is found to be more useful in yielding *bulk* informations on the developing glide polygonization, *at the sample scale.*

In section 2 the different experimental procedures are described ; our results are presented in section 3 ; and section 4 is devoted to their interpretation.

2. **Experimental procedures.** — 2.1 PLASTIC DEFORMATION AND THERMAL ACTIVATION PARAMETERS. — A large *as-grown* single crystal ($300 \times 35 \times 1.2$ mm^3) was supplied by IRSID. It contained about 100 ppm (ωt) carbon and 20 ppm (ωt) nitrogen.

Tensile samples were mechanically cut from it using a gauge to obtain a Schmid factor on the $(\bar{1}01)$ [111] slip system about 0.5, with dimensions 14 mm × 3 mm^2.

Specimens were then chemically polished and purified by annealing in wet hydrogen, first at 550 °C for 16 hours, then at 720 °C for 24 hours, and finally in dry hydrogen at 720 °C for 9 hours. Snoek internal friction analyses gave a carbon content reduced to 10 ppm (ωt) and a nitrogen content reduced to 5 ppm (ωt).

Tensile tests were conducted in an Instron machine imposing a constant shear strain rate of $\dot{\gamma} = 2.5 \times 10^{-5}$ s^{-1}.

Creep tests were performed in tension using a weight machine built in the laboratory [18]. The specimen is deformed in the machine itself up to a given shear stress, then it is allowed to creep for some time. In between the different creep runs, weights are added in order to keep as nearly as possible a shear strain rate equal to that in the Instron tests. Controlled temperature baths (ethyl-alcohol or isopentane) are used at 295, 250, 225, 200, 173, 150 and 123 K. The temperature of the sample is given accurately by a thermocouple attached to it.

The resolved shear stress τ and the strain γ are calculated from the appropriate single-slip formula [15].

Activation volumes (v/b^3) are obtained by using the stress relaxation technique [16]. At 150, 200, 225 and 250 K they are also measured by stress changes during creep tests.

Activation energies are measured by differential temperature changes during creep tests. The shape of the creep curves $\gamma(t)$ is very often found to be linear; when logarithmic, they are resolved by a method similar to the one used for stress-relaxation tests [16, 18].

2.2 THE BERG-BARRETT METHOD. — In order to facilitate the understanding of X-ray topographs the origin of the observed contrasts is briefly recalled. Defects in a crystal give rise to two kinds of contrast [9]:

1) *Extinction contrast* : a defect (dislocation) decreases locally the primary extinction which is due to destructive interference [9]. On the topographs, contrast lines appear as black lines on a grey background.

2) *Misorientation contrast* : this results from local rotations of the lattice (as produced by subgrain boundaries for example).

This contrast allows one to appreciate in a given dislocation wall those dislocations which equilibrate their sign (i. e. producing balanced + and − lattice rotation) from those which are in excess and produce the net misorientation across the wall. This can be shown easily when decomposing the lattice rotation axis into its three components.

Let β be the component of rotation about the intersection of the reflecting and the incident planes. The incident angle varies slowly with β as $\delta\theta \sim 0.5\ \beta^2$. Usually the strain-induced β component is smaller than one degree, making $\delta\theta$ smaller than one minute i. e. smaller than the actual value of the Bragg width $\Delta\theta$ used in our apparatus. Thus the X-ray beam is still reflected. It is merely deviated by a displacement Δy on the film, perpendicular to the incident plane and equal to $2\ \beta\ D' \sin\theta$ where D' is the crystal-film spacing. Now assume the wall to be merely a kink wall : then the X-ray beam images onto the film a symmetrical cusp-shaped contrast, the so-called *displacement contrast* (Fig. 14).

Let us now consider the rotation component γ, about the normal to the incident plane. This component changes the incident angle directly. As soon as γ exceeds $\Delta\theta$, it brings the crystal out of contrast, hence producing a black-white contrast, the so-called *orientation contrast* (Fig. 15). This contrast is quite useful to display the net lattice misorientation across a wall.

Finally the last component lies about the normal to the reflecting plane, and leaves the incident angle unchanged ; it is therefore completely neutral and causes no additional contrast.

In short, an analysis of Berg-Barrett contrasts allows us to estimate the kink character and the misorientation character of cell walls formed during straining by glide polygonization.

In our experiments we used the linear focus (7×0.07 mm^2) of a Cr anticathode ($\lambda_{K_\alpha} \simeq 2.29$ Å) in the following conditions : $V = 50$ kV, $I = 7.5$ mA. After deformation, a lamella $10 \times 3 \times 1$ mm^3 is cut chemically from the middle part of specimen, where the deformation is the most homogeneous. After acid-polishing it is topographied on the two different surfaces : the (001) face, i. e., the lamella plane, and the $(1\bar{2}0)$ face, i. e., the edge plane. The

reflections used are : $\mathbf{g} = (001)$ for the (001) face and $\mathbf{g} = (0\bar{1}0)$ or $(1\bar{1}0)$ for the $(1\bar{2}0)$ face.

Indeed, in our case, only three kinds of reflection satisfy the Bragg relation $\lambda = 2\,d \sin\theta$:

$$\mathbf{g} = \langle\, 110 \,\rangle$$
$$\mathbf{g} = \langle\, 200 \,\rangle$$
$$\mathbf{g} = \langle\, 211 \,\rangle\,.$$

The $\langle\, 211 \,\rangle$ reflections have been omitted because of their relatively weak structure factor and of their large Bragg angle ($\theta \simeq 77°$) [8]. Among the $\langle\, 110 \,\rangle$ and $\langle\, 200 \,\rangle$ reflections, only $\mathbf{g} = (001)$ for the (001) face and $\mathbf{g} = (1\bar{1}0)$ or $(0\bar{1}0)$ for the $(1\bar{2}0)$ face are allowed, because the other ones would have a reflecting plane too much inclined relative to the face topographied.

3. **Results.** — Our study was limited by two factors :

— the occurence of profuse twinning at 150 K and below,

— the tendency to necking at lower temperatures.

A low-shear strain rate $\dot{\gamma} = 2.5 \times 10^{-5}\ s^{-1}$ was chosen to limit twinning. In spite of this, the specimen tested at 123 K, had to be prestrained 5 % at 180 K in order to obtain a sufficient shear strain.

X-ray analyses of the tensile-axis rotation for all the specimens show that slip occurs predominantly on the primary slip system. As has often been observed [10], the conjugate slip system (101) $[\bar{1}11]$, also noticed on our X-ray topographs, produces only a local deformation and does not play much part in the macroscopic deformation.

It is clear that some transition temperature occurs near 200 K in the observed plastic behaviour of α-iron, as has been incidentaly reported by some authors [17]. Roughly speaking, some kind of dynamic recovery already starts, being noticeable at higher temperatures. We detail this phenomenon below, dividing our observations into three ranges relative to that temperature.

3.1 HIGH-TEMPERATURE RANGE. — 3.1.1 *Plastic deformation.* — The deformation behaviour is characterized by :

(i) A constant work-hardening rate during a test. From the first percents of strain it reaches 6 kg/mm² at 296 K and 10 kg/mm² at 250 K (Fig. 1, 2).

The sample used in the tensile test at 225 K does not come from the same as-grown crystal as the other ones ; the corresponding stress-strain curve presents a yield point which is probably due to a slightly larger content of interstitial carbon. This yield point could not be eliminated by a slow cooling from the annealing temperature. However, above 10 % shear strain the work-hardening rate becomes constant (6 kg/mm²) as in other samples (Fig. 3).

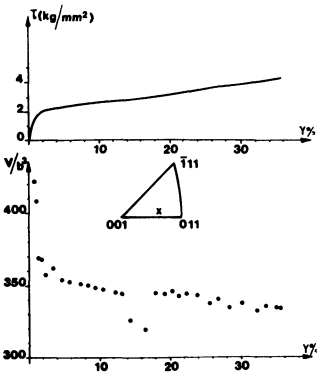

FIG. 1. — T = 296 K { Resolved shear stress-strain curve $\dot{\gamma} = 2.5 \times 10^{-5}\ s^{-1}$. Activation volume ($v/b^3$) versus resolved shear strain.

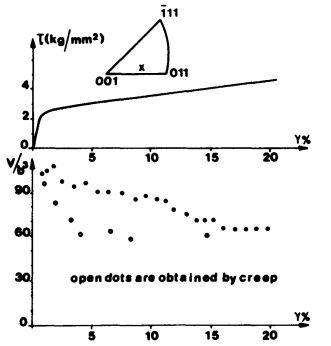

FIG. 2. — T = 250 K { Resolved shear stress-strain curve $\dot{\gamma} = 2.5 \times 10^{-5}\ s^{-1}$. Activation volume ($v/b^3$) versus resolved shear strain.

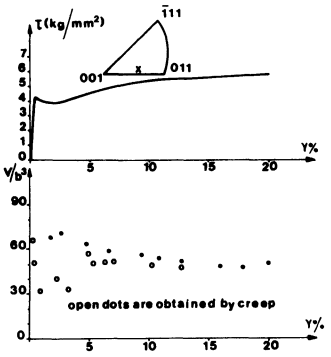

FIG. 3. — T = 225 K { Resolved shear stress-strain curve $\dot{\gamma} = 2.5 \times 10^{-5}\ s^{-1}$. Activation volume ($v/b^3$) versus resolved shear strain.

The elastic limits are still thermally activated and in agreement with those measured by other authors [5, 17].

(ii) Activation volumes decrease with increasing strain (Fig. 1, 2, 3). For a 20 % shear strain the decrease is about 30 b^3. At room temperature activation volumes are rather large (350 b^3), as a consequence of the small shear-strain rate. As has already been observed [17], they increase very fast with increasing temperature or decreasing strain rate.

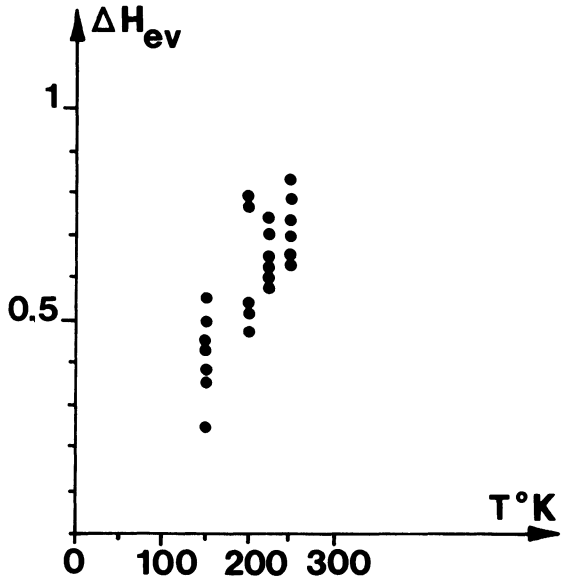

FIG. 4. — Activation energy versus temperature.

They depend also on the nature of the test : volumes measured by stress change in the creep test are definitely different from those measured by stress relaxation, and in contrast with these they remain constant during the deformation. At lower temperatures (225 K) this difference becomes smaller, but does not vanish.

(iii) Activation energies level off with temperature to about 0.8 eV instead of being proportional to it (Fig. 4).

3.1.2 X-*Ray observations.* — The whole set of topographs (figures 5 → 10) reveals two kinds of dislocation entanglements :

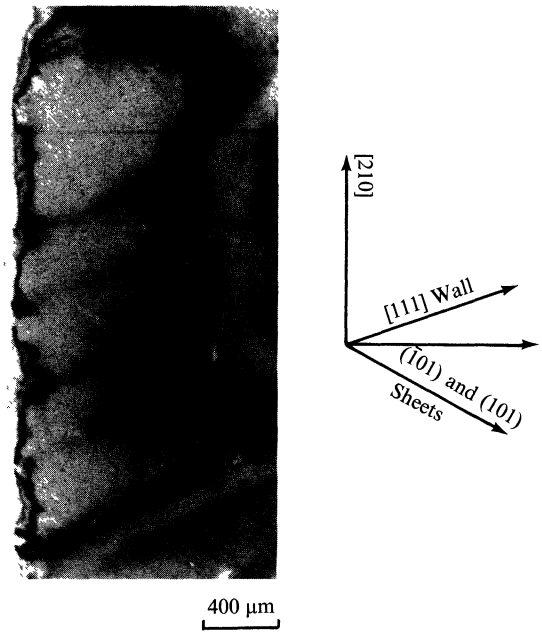

FIG. 5. — T = 250 K — γ = 8 % (001) face — **g** = [001]
{ orientation axis : [210]
{ displacement axis : [1$\bar{2}$0].

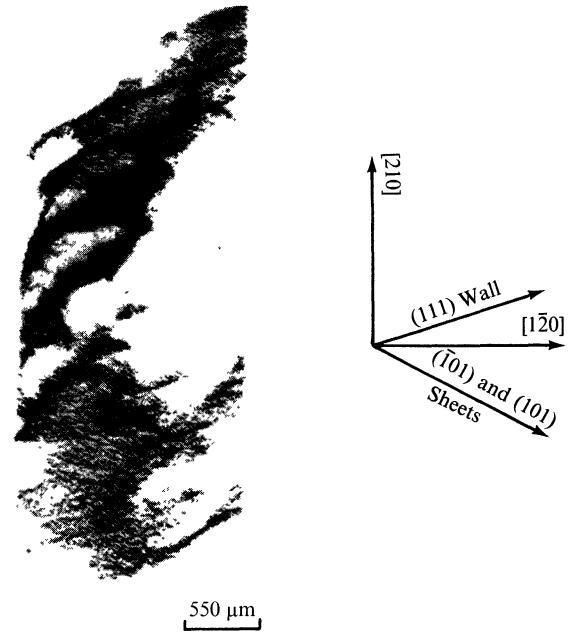

FIG. 6. — T = 250 K — γ = 20 % (001) face — **g** = [001]
{ orientation axis : [210]
{ displacement axis : [1$\bar{2}$0].

(i) Rough dislocation walls parallel to (1$\bar{1}$1) planes, with alternate lattice tilts around the [1$\bar{2}$1] primary edge direction. The distance between two consecutive walls is rather large ; at 250 K it is of the order of 500 μm for 8 % strain (Fig. 5) and goes down to 200 μm for 20 % strain (Fig. 6). Furthermore it is nearly independent of temperature.

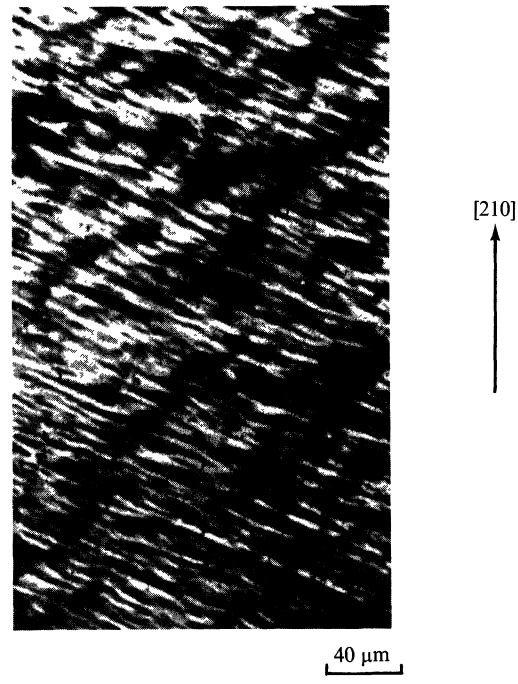

FIG. 7. — T=250 K — γ=20 %. Slip lines on (001) face observed by optical microscopy.

FIG. 8. — T = 250 K — γ = 20 % (001) face — $\mathbf{g}$ = [001]
{ orientation axis : [1$\bar{2}$0]
{ displacement axis : [210].

FIG. 9. — T = 250 K — γ = 20 % (1$\bar{2}$0) face — $\mathbf{g}$ = [0$\bar{1}$0]
{ orientation axis : [001]
{ displacement axis : [100].

(ii) Dislocation sheets, roughly stretched along ($\bar{1}$01) active slip lamellae and (101) conjugated ones. They induce both a lattice tilt and a lattice kink around the axis $\mathbf{\Omega}_s$ = [1 $\bar{1}$ l]. They are close together, in a one-to-one correspondance with slip lines (Fig. 7).

These conclusions are based on the following topographic analysis :

(i) Nuclear plate analysis shows that :

• The axis $\mathbf{\Omega}_\perp$ has no component in the [210] direction : there is no rotation contrast on (001) topographs; the (111) walls occur here mainly by extinction contrast (Fig. 5, 6).

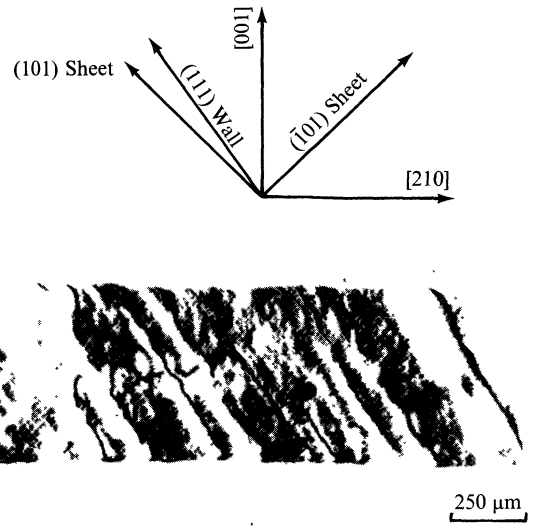

FIG. 10. — T = 250 K — γ = 20 % (1$\bar{2}$0) face — $\mathbf{g}$ = [1$\bar{1}$0]
{ orientation axis : [001]
{ displacement axis : [110].

• $\mathbf{\Omega}_\perp$ has a non-vanishing component in the [1$\bar{2}$0] direction : when the crystal is rotated by 90° (Fig. 8), the corresponding topograph shows an important rotation contrast.

• $\mathbf{\Omega}_\perp$ has also a component in the [001] direction : on the (1$\bar{2}$0) face the walls appear by rotation contrast in both reflections : $\mathbf{g}$ = [0$\bar{1}$0] (Fig. 9), and $\mathbf{g}$ = [1$\bar{1}$0] (Fig. 10).

The most reasonable lattice rotation compatible with these contrasts is about the [1$\bar{2}$1] direction.

(ii) The ($\bar{1}$01) and (101) sheets are mainly revealed on the (1$\bar{2}$0) topographs. The best observations can be taken from topographs after deformation at 200 K (see below), but already at 250 K the following features can be noticed :

• The $\mathbf{\Omega}_s$ axis has no component along the [110] direction : the displacement contrast, induced by the sheets and clearly visible on the (0$\bar{1}$0) reflection (Fig. 9), vanished on the (1$\bar{1}$0) reflection (Fig. 10).

• $\mathbf{\Omega}_s$ has a component along [001], since a strong rotation contrast occurs along the sheet traces, on both the above-mentioned reflections (Fig. 9, 10).

Only a [1$\bar{1}$ l] axis, with $l \neq 0$, fits these observations. Also, this sheet rotation causes the right rotation contrasts which are observed on (001) topographs (Fig. 6). But the occurence of displacement contrasts on some (1$\bar{2}$0) topographs is evidence for a kink character in the sheets, i. e., for the existence of numerous + and − dislocations inside.

3.2 TRANSITION RANGE. — 3.2.1 *Plastic deformation.* — At T = 200 K there is a transition in the plastic behaviour :

— Above about 10 % strain, the work-hardening rate goes down to zero (Fig. 11).

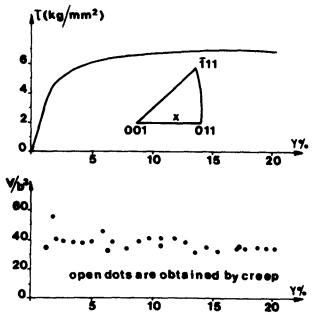

FIG. 11. — T = 200 K { Resolved shear stress-strain curve $\dot{\gamma} = 2.5 \times 10^{-5}\ s^{-1}$. Activation volume ($v/b^3$) versus resolved shear strain.

— Activation volumes are nearly constant; they have the same value in creep test as in the relaxation test (Fig. 11).

— Activation energies are independent of strain and have a value of about 0.8 eV (Fig. 4).

3.2.2 X-*ray observations.* — The dislocation substructure is now quite different :

— They are no more (111) walls.

— On the contrary, sheets are still present; however, they are more widely spaced than previously, about in a one-to-ten correspondence with slip lines (Fig. 12). Their spacing is now about 30 μm, instead of 10 μm at 250 K (Fig. 13). They form here the only existing structure, so that they can be best studied. In addition to the features observed at 250 K, some visible fine structure can be noted here.

On the (001) face many cross-slip traces are visible. Most of them appear perpendicularly to the slip lines (A Fig. 13), they are consistent with primary and conjugate cross-slip on the common (0$\bar{1}$1) cross slip plane.

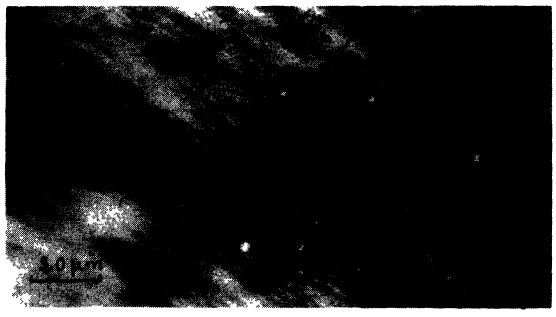

FIG. 12. — T = 200 K — γ = 20 %. Slip lines on (001) face observed by optical microscopy.

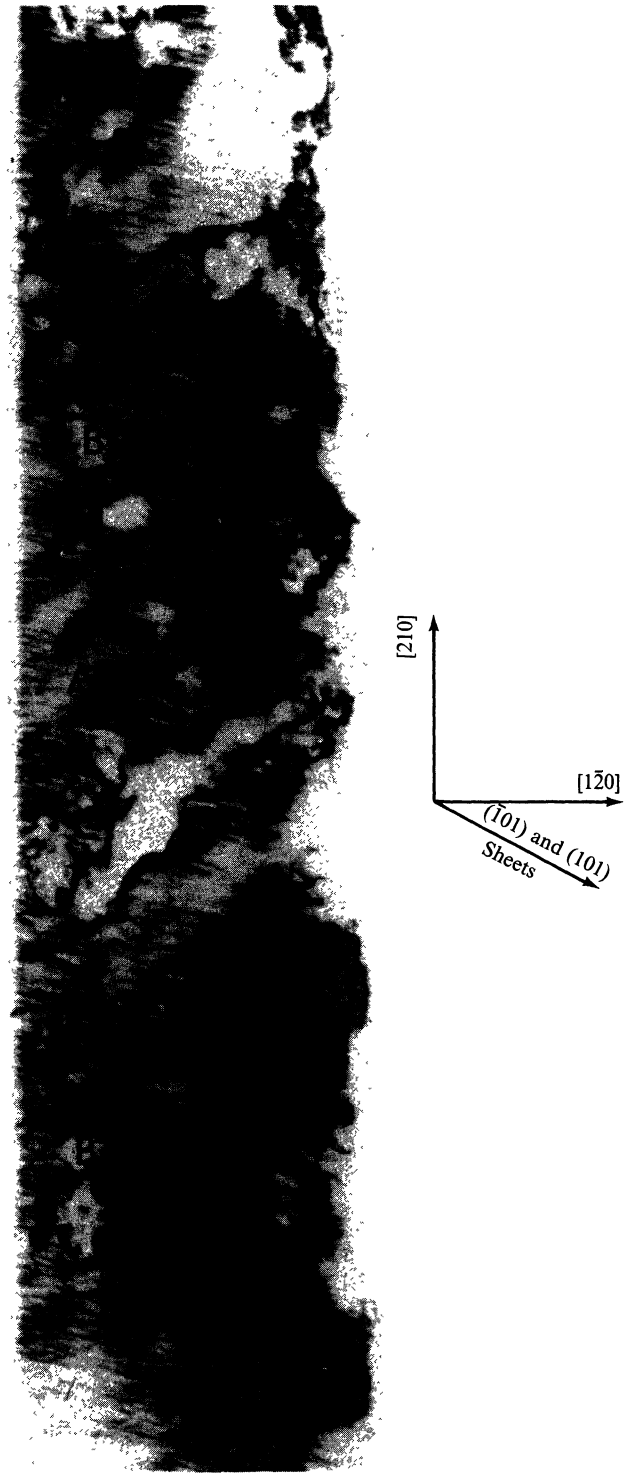

FIG. 13. — T = 200 K — γ = 20 % (001) face — **g** = [001] { orientation axis : [210] displacement axis : [1$\bar{2}$0].

Some others, inclined at an angle of 18° relatively to the slip lines, occur horizontally on the topographs (B, Fig. 13); they denote cross-slip on the (211) plane.

On the (1$\bar{2}$0) face, with (0$\bar{1}$0) reflection (Fig. 14), X-ray displacement Δy, as produced by a kink β around the [100] axis, can be measured. By means of the above mentioned relation, $\Delta y = 2\,\beta D' \sin\theta$ (§ 2.2.2), β is easily estimated. In our experiment the film is mounted at a distance D' of about 1 mm from the crystal surface; thus we find a kink component of about 15′. By electron microscopy Foxall *et al.* [10] measured rotations of the same order in niobium single crystals deformed at room temperature.

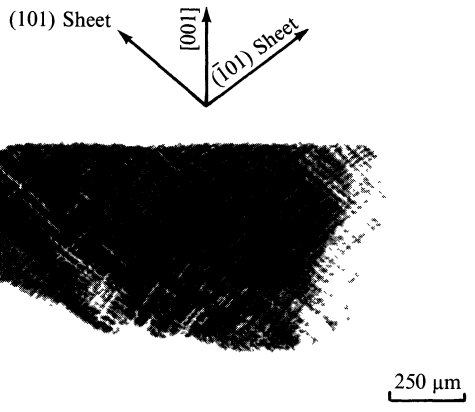

FIG. 14. — $T = 200$ K — $\gamma = 20\ \%$ $(1\bar{2}0)$ face — $\mathbf{g} = [0\bar{1}0]$
{ orientation axis : [001]
{ displacement axis : [100].

FIG. 15. — $T = 200$ K — $\gamma = 20\ \%$ $(1\bar{2}0)$ face — $\mathbf{g} = [1\bar{1}0]$
{ orientation axis : [001]
{ displacement axis : [110].

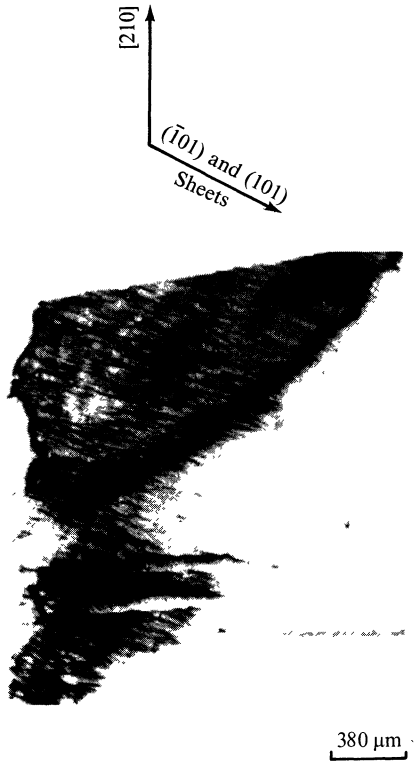

FIG. 16. — $T = 200$ K — $\gamma = 8\ \%$ (001) face — $\mathbf{g} = [001]$
{ orientation axis : $[210]$
{ displacement axis : $[1\bar{2}0]$.

Furthermore, as is shown on the topographs (Fig. 13, 16), the dislocation substructure built up after 8 % strain is similar to the one observed after 20 % strain.

3.3 LOW-TEMPERATURE RANGE. — 3.3.1 *Plastic deformation.* — This is characterized by :

(i) Low work-hardening rates (Fig. 17, 18, 19).

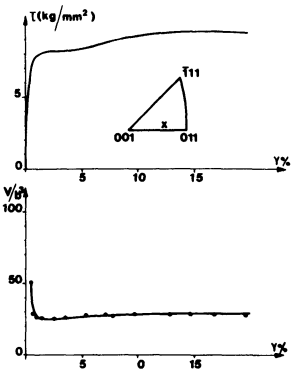

FIG. 17. — $T = 173$ K { Resolved shear stress-strain curve
$\dot{\gamma} = 2.5 \times 10^{-5}\ s^{-1}$.
Activation volume (v/b^3) versus resolved shear strain.

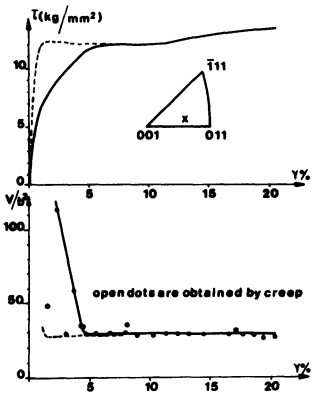

FIG. 18. — $T = 150$ K { Resolved shear stress-strain curve
$\dot{\gamma} = 2.5 \times 10^{-5}\ s^{-1}$.
Activation volume (v/b^3) versus resolved shear strain.

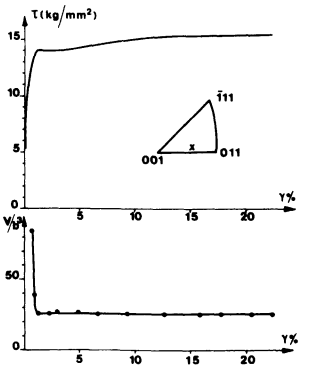

FIG. 19. — $T = 123$ K { Resolved shear stress-strain curve
$\dot{\gamma} = 2.5 \times 10^{-5}\ s^{-1}$.
Activation volume (v/b^3) versus resolved shear strain.

(ii) Activation volumes depend neither on strain nor on the nature of the test : they are only functions of the stress. The values obtained at the elastic limit are in good agreement with those measured by other authors [7, 17].

(iii) Activation energies are independent of strain, but they vary proportionally with the temperature (Fig. 14).

3.3.2 X-*ray observations.* — The $(\bar{1}01)$ and (101) sheets fade out.

On the $(1\bar{2}0)$ face, at 20 % strain, there are no more visible rotations and no displacement contrasts (Fig. 20). Only the two-slip system traces are noticeable, probably by a slight extinction contrast.

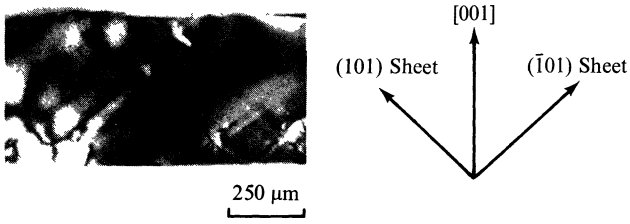

FIG. 20. — T = 150 K — γ = 20 % $(1\bar{2}0)$ face — $\mathbf{g} = [0\bar{1}0]$
{ orientation axis : [001]
{ displacement axis : [100].

On the (001) face (Fig. 21) the extinction contrasts, produced by incidental sheets, are hardly detected.

At 8 % strain there is no more lattice rotation throughout the crystal.

3.3.3 *Prestrain.* — The only effect of prestraining on the $\tau(\gamma)$ curves is to suppress the more or less extensive preyield stages which are visible on the stress-strain curves of annealed samples.

The curves $\tau(\gamma)$ are the same in shape and the thermal activation parameters are unchanged.

However, comparing figure 22 to figure 23 shows that the substructure built up during prestraining at 180 K has been only weakly changes by further deformation at 123 K. Even for the much larger stresses experienced at this temperature the sheets do not disappear, which proves the great stability

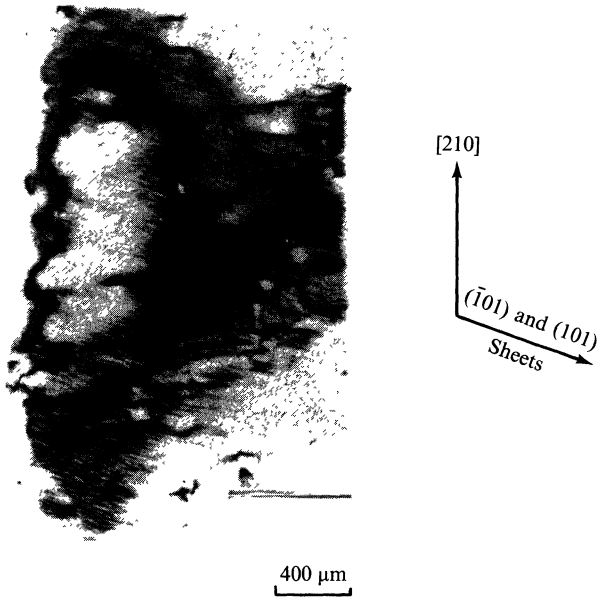

FIG. 22. — T = 123 K — γ = 20 % (001) face — $\mathbf{g} = [001]$
{ orientation axis : [210]
{ displacement axis : [1$\bar{2}$0].

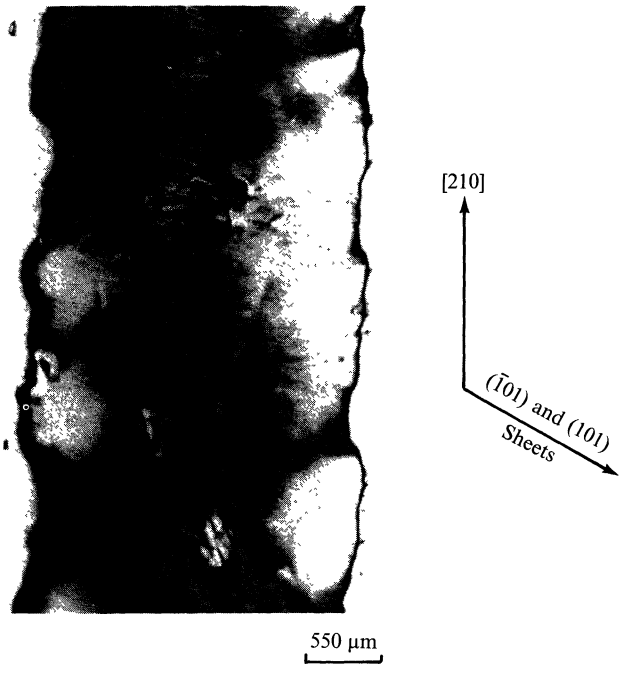

FIG. 21. — T = 150 K — γ = 20 % (001) face — $\mathbf{g} = [001]$
{ orientation axis : [210]
{ displacement axis : [1$\bar{2}$0].

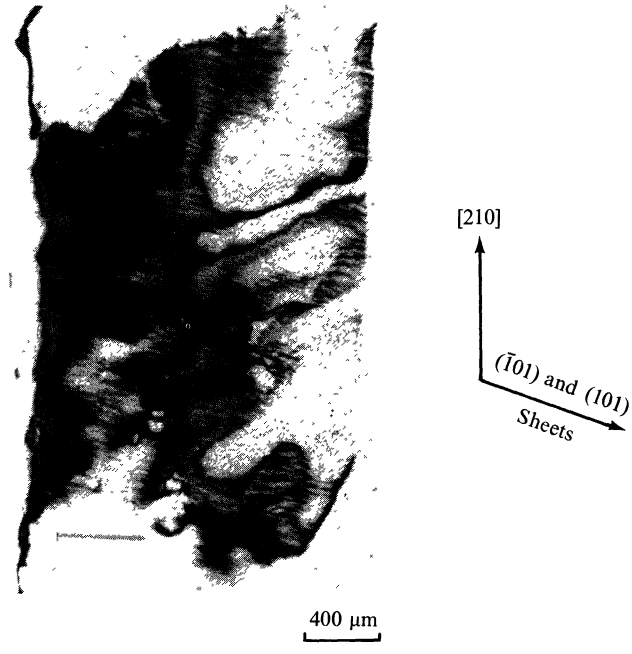

FIG. 23. — T = 173 K — γ = 20 % (001) face — $\mathbf{g} = [001]$
{ orientation axis : [210]
{ displacement axis : [1$\bar{2}$0].

of these entanglements. It also shows that substructure observations on prestrained samples must always be considered with some caution : they might be more typical of the prestrain temperature than of the actual test temperature.

4. **Interpretation and discussion.** — 4.1 NATURE OF THE ENTANGLEMENTS OBSERVED ABOVE 200 K. — Two kinds of entanglements are revealed for our stress orientation :

(i) (111) walls consisting of primary edge dislocations. They are probably built up by the mutual capture of dislocations. As kink walls do, they give rise to alternate tilts around the direction $[1\bar{2}1]$.

At the strain levels studied they are too widely spaced to play an important role in the plastic behaviour.

(ii) Sheets extending on primary and conjugate slip planes. They give rise to a much finer structure. They probably result from interaction between primary and conjugate screws and exert a great influence on the strengthening mechanism.

Thus, there is cause to discuss their detailed nature and the way they build up.

During plastic deformation the dislocation substructure generally develops in order to screen out the long-range stress fields which are induced by this substructure itself : this is the slip polygonization. This screening out cannot be perfect without dislocation climb, that is to say at low temperature. Up to a point, the cross-slipping of screws (which is easy in b. c. c. metals) helps to obtain a better screening out or a finer polygonization.

At all events, this is a good way to describe possible interactions between dislocations during deformation : to look for what the nature of perfect slip polygonization should be, even if we know that it will be only crudely built up.

It is easy to carry out this study with the help of the Frank formula [11]. Suppose that dislocations are not allowed to climb and let us consider only the two following dislocation families :

1) One family of $\frac{1}{2}\langle 111 \rangle$ primary dislocations and one family of $\frac{1}{2}\langle 11\bar{1} \rangle$ conjugate dislocations.

TABLE I

Possible subgrain boundaries without long-range stress field in iron
Ω *is the subgrain boundary rotation axis and* **v** *its normal*

Two families : $\mathbf{b}_1 = \frac{1}{2}[111]$ and $\mathbf{b}_2 = \frac{1}{2}[\bar{1}11]$

(1) parallel dislocations

[a] different slip planes : $(\bar{1}01)$ and (101)

TILT $\begin{cases} \boldsymbol{\Omega} = [010] \\ \mathbf{v} = [100] \end{cases}$

dislocations line // [010]

[b] identical slip plane : $(0\bar{1}1)$

TILT $\begin{cases} \boldsymbol{\Omega}.\mathbf{v} = 0 \\ \mathbf{v} = [\rho_1 - \rho_2, \rho_1 + \rho_2, \rho_1 + \rho_2] \end{cases}$

with $\begin{bmatrix} \rho_1 : \text{dislocations 1 density} \\ \rho_2 : \text{dislocations 2 density} \end{bmatrix}$

(2) non parallel dislocations

[a] different slip planes : $(\bar{1}01)$ and (101)

MIXED $\begin{cases} \boldsymbol{\Omega} = [0\bar{1}1] \\ \mathbf{v} = [010] \end{cases}$

dislocations 1 line // [101]
dislocations 2 line // $[\bar{1}01]$

[b] identical slip plane : $(0\bar{1}1)$

TWIST $\begin{cases} \boldsymbol{\Omega} = [0\bar{1}1] \\ \mathbf{v} = [0\bar{1}1] \end{cases}$

Two families : $\mathbf{b}_1 = \frac{1}{2}[111]$ and $\mathbf{b}_3 = [100]$

(1) parallel dislocations

[a] different slip planes : $(\bar{1}01)$ and $(0\bar{1}1)$

TILT $\begin{cases} \boldsymbol{\Omega} = [111] \\ \mathbf{v} = [\bar{2}11] \end{cases}$

dislocations line // [111]

[b] identical slip plane : $(0\bar{1}1)$

TILT $\begin{cases} \boldsymbol{\Omega}.\mathbf{v} = 0 \\ \mathbf{v} = [\rho'_1 + 2\rho_3, \rho'_1, \rho'_1] \end{cases}$

with $\begin{bmatrix} \rho'_1 : \text{dislocations 1 density} \\ \rho_3 : \text{dislocation 3 density} \end{bmatrix}$

(2) non parallel dislocations

[a] different slip planes : $(\bar{1}01)$ and $(0\bar{1}1)$

MIXED $\begin{cases} \boldsymbol{\Omega} = [0\bar{1}1] \\ \mathbf{v} = [\bar{1}0\bar{2}] \end{cases}$

dislocations 1 line // [010]
dislocations 3 line // $[\bar{2}11]$

[b] identical slip plane : $(0\bar{1}1)$

TWIST $\begin{cases} \boldsymbol{\Omega} = [0\bar{1}1] \\ \mathbf{v} = [0\bar{1}1] \end{cases}$

2) One family of $\langle 100 \rangle$ dislocations and one of $\frac{1}{2}\langle 111 \rangle$ dislocations. $\langle 100 \rangle$ dislocations are produced by interactions of primary and conjugate screws [10] such as :

$$\tfrac{1}{2}[111] + \tfrac{1}{2}[1\bar{1}\bar{1}] = [100] .$$

Then all possible combinations of these families into boundaries without long-range stresses are summarized in table I.

Experimentally the sub-boundary rotation axis is observed to be parallel to the $[1\bar{1}\, l]$ direction, $l \neq 0$ (§ 3.1.2). Comparing with table I, this rules out any sub-boundaries with a twist component. The only compatible situation is obtained with 1(b) configurations, a pure tilt case with boundary plane of the type (h, k, k) and rotation axis at the intersection of the *common* slip plane $(0\bar{1}1)$ and the boundary plane, i. e., parallel to $[-2k, h, h]$. Identifying with $[1\bar{1}\, l]$, the direction found experimentally, yields $h = 2k$, i. e., a $[\bar{1}11]$ tilt boundary with boundary plane of the type (211). Dislocation densities in the sub-boundary follow from its [211] normal direction. Finally two configurations are possible as the final product of glide polygonization :

(i) Sub-boundaries consisting of parallel [100] dislocations combined with parallel primary dislocations, with one [100] for every two $\frac{1}{2}[111]$.

The formation of these sub-boundaries can be explained as follows : at temperatures high enough for the lattice friction to be sufficiently low, primary and conjugate screws can rearrange in the common cross-slip plane $(01\bar{1})$ in order to screen out their long-range stresses. This is likely to occur in our case because stress orientation helps slipping in that $(01\bar{1})$ plane, the Schmid factor of which is still half of the value in primary slip plane, i. e., 0.25 (see § 4.3). It explains the numerous prominent cross-slips observed on a large scale on (001) faces (A, Fig. 13). It is worth noting here that primary dislocations have to cross slip into loops long enough to be mobile in that plane in order to feed the growing sub-boundary.

(ii) Sub-boundaries may also consist of only primary and conjugate dislocations, with one conjugate for every three primary ones. This case is not really different from the one above ; conjugate and primary dislocations here have just not reacted, having cross-slipped on parallel but different $(01\bar{1})$ planes.

According to our observations, sheets are mainly stretched along the primary and conjugate slip planes (Fig. 14, 15). They appear only locally along the trace of the (211) plane, and over small distances (B, Fig. 13). This shows how far from perfect is the so-formed slip polygonization, and emphazizes the local character of the sub-boundaries described. Consequently, they have to produce some long-range stresses. These configurations may be better defined as *multipoles*, referring to their kink character as noted above. Their formation and stability have been already studied in other contexts, for example, by Hazzledine [12].

4.2 Connections with activation parameters. — At low temperatures the high lattice friction prevents any dislocation rearrangement. Primary and conjugate screws are not allowed to interact so that, on the X-topographs (Fig. 20, 21), sheets and lattice misorientations disappear : the two slip systems behave independently.

Accordingly, the corresponding stress-strain curves (Fig. 17, 18, 19) show only a slight hardening, probably due to trails and other debris left behind in the wake of screws [7, 14, 1].

Activation volumes are function of stress alone, and activation energies are linear in temperature. Both are constant at a given temperature. This suggests strongly that the same mechanism controls the flow stress from the elastic limit to the largest strain. The whole plasticity is governed by the interaction between screw dislocations and the crystal lattice.

On the contrary, at higher temperatures, screw rearrangements produce sheets ; these introduce, at the same time, new dislocations sources [1] and obstacles to dislocation glide. Consequently, as the stress increases, the screw density $\rho_m(\tau)$ should increase very fast initially, then more and more slowly as obstacles multiply and stop numerous screw dislocations ; i. e.,

$$\frac{\partial \rho_m}{\partial \tau} > 0 ; \qquad \frac{\partial^2 \rho_m}{\partial \tau^2} < 0 . \tag{1}$$

This simple model is sufficient to explain the observed activation parameters behaviour. It shows that the *apparent* measured activation volume is larger than the true one and that the activation energy varies much more slowly with temperature.

The glide velocity of the thermally activated dislocations produces a shear strain rate of the crystal :

$$\dot{\gamma} = \dot{\gamma}_0 \exp\left(-\frac{\Delta G}{kT}\right),$$

in which $\dot{\gamma}_0$ depends on ρ_m : $\dot{\gamma}_0 = C\rho_m$, where ρ_m is a function of γ, i. e., of τ. This enables us to write :

$$\dot{\gamma} = C\rho_m \exp\left(-\frac{\Delta G}{kT}\right) \text{ or } \Delta G = kT \ln\left(\frac{C\rho_m}{\dot{\gamma}}\right). \tag{2}$$

As ρ_m increases rapidly with increasing stress, so does the strain rate $\dot{\gamma}$; accordingly the *apparent* activation volume :

$$V_{app} = kT\left(\frac{\partial \ln \dot{\gamma}}{\partial \tau}\right)_{T,str.} \tag{3}$$

is larger than the true one $V = -\partial \Delta G/\partial \tau$.

On the other hand, as T increases, the flow stress at a given dislocation substructure decreases ; according to relation (1) the density $\rho_m(\tau)$ does likewise ; then it follows from eq. (2) that ΔG increases more and more slowly with increasing temperature.

One can write :

$$V_{app} = -\frac{\partial \Delta G}{\partial \tau} + kT\frac{\partial \ln \rho_m}{\partial \tau} = V + kT\lambda \quad (4)$$

with

$$\lambda(T) = \left(\frac{\partial \ln \rho_m}{\partial \tau}\right)_{T,str.}$$

$$\left(\frac{\partial V_{app}}{\partial \gamma}\right)_{T,\dot{\gamma}} = kT\theta\left(\frac{\partial^2 \ln \rho_m}{\partial \tau^2}\right),$$

$$\text{where} \quad \theta = \left(\frac{\partial \tau}{\partial \gamma}\right)_{\dot{\gamma},T}. \quad (5)$$

Note that ΔG derivatives have not to appear in relation (5). This is because the flow stress decomposes into two components :

$$\tau = \tau^*(T) + \tau_i(\tau, \gamma)$$

where τ^* is the thermal component and τ_i the athermal one. Any strain variation leads to a variation of τ only through τ_i : $d\tau = d\tau_i$, while ΔG is a function of τ^*, i. e., of T.

It is of interest to notice that the *apparent* variations of ΔG also depend on the additional term λ :

$$\left(\frac{\partial \Delta G}{\partial T}\right)_{\dot{\gamma},str.} = k \ln \frac{\dot{\gamma}_0}{\dot{\gamma}} + kT\lambda\left(\frac{\partial \tau}{\partial T}\right)_{\dot{\gamma},str.} \quad (6)$$

and

$$\left(\frac{\partial \Delta G}{\partial \gamma}\right)_{T,\dot{\gamma}} = kT\lambda\theta\,. \quad (7)$$

Eq. (1), (4), (5) show how the curves $V_{app}(\gamma)$ obtained at 296, 250 and 225 K, represent the function $\rho_m(\tau)$.

At 250 K, for example, the apparent behaviour of the activation volume as shown in figure 2 is consistent with a screw density which satisfies eq. (1), and seems to reach a maximum above 20 % strain. More explicitly, any reasonable relation chosen between ρ_m and τ, such as :

$$\rho_m(\tau) = \rho_0 + \left(\frac{\tau - \tau_0}{\mu b}\right)^2,$$

yields a difference $(V_{app} - V)$ of the right order of magnitude $(30\,b^3)$ [18].

The observed values of the variations of ΔG with T or γ are also in good agreement with this model.

On that basis, the comparison between creep and relaxation measurements means that screw multiplication may be very dependent on the nature of the test, here a creep test as opposed to a constant strain-rate test.

Relation (6) predicts a decrease of the slope of $\Delta G(T)$ at higher temperature : at 250 K, with

$$kT\lambda = V_{app} - V = 30\,b^3$$

at the elastic limit and

$$\left(\frac{\partial \tau}{\partial T}\right)_{\dot{\gamma},str.} \simeq -4 \times 10^{-2}\ \text{kg/mm}^2\,.\,\text{K}\,,$$

we obtain a reduction of the slope of $\Delta G(T)$ by one third.

On the other hand, relation (7) gives an almost zero variation of ΔG with the shear strain γ, as is observed (Fig. 4) : at $T = 250$ K, $\theta = 10$ kg/mm^2 and $kT\lambda = 30\,b^3$, it yields an increment of 0.25×10^{-2} eV for one percent strain.

4.3 MEANING OF THE TRANSITION TEMPERATURE $T = 200$ K. — We now discuss why the transition occurs at about 200 K and what the meaning of this temperature is.

In contrast with the high-temperature case the lattice friction is preponderant below 200 K and prevents any dislocation cross-slip on a large scale.

So, in this model, $T = 200$ K represents the temperature at which a screw dislocation can still cross-slip off its slip plane over a sufficient length.

Such a cross-slip can be represented in two different ways :

1) Two opposite screw dislocations on parallel primary slip planes a distance d apart attract each other, deviate on the common cross-slip plane, and annihilate, leaving in this plane two primary edge debris along $[\bar{2}11]$. Because of their high mobility, they can then rearrange in order to relax their internal stresses.

Screws can deviate only if the combined effect of their mutual attraction *and* the applied stress (resolved on the common cross-slip plane) is larger than the lattice friction in this plane [19], that is to say :

$$\tau \cos\theta + \frac{\mu b \sin\theta}{2\pi d} \geqslant \tau$$

where τ is the applied stress, resolved in the common cross-slip plane and measured at the elastic limit, and θ the angle between the slip plane and the cross-slip plane.

At the transition temperature the two terms should be equal ; so we obtain the distance d between two consecutive active planes :

At 200 K, we have :

$$\begin{cases} \tau = 5\ \text{kg/mm}^2 \\ \mu = 2\,000\ \text{kg/mm}^2 \\ \theta = 45^\circ \end{cases}$$

which gives us :

$$d \simeq 650\, b\,; \quad \text{i. e.,} \quad \underline{d \simeq 0.11\ \mu\text{m}}\,.$$

2) The primary screws cross-slip in $(01\bar{1})$ plane can alternatively be driven by the trapping of these ones in a forming dislocation sheet. Sketching this latter as a growing sub-boundary in a (211) plane, the long-range stresses exerted by the sheet on a dislocation are roughly given by [13] :

$$\sigma \simeq \frac{\mu b}{2\,\pi d}$$

where d is now the average spacing of dislocations in the multipole. So this argument leads to an equation identical with the previous one and to a nearly equal value of d. Here, this value yields a lattice misorientation across the sub-boundary $\Omega \simeq b/d \simeq 3 \times 10^{-3}$ rad, i. e., about 10′. This is in good agreement with our experimental observations (§ 3.2.2).

5. **Conclusion.** — Our results show that the Berg-Barrett technique is a very convenient tool for following the evolution of the dislocation substructure, even up to 20 % or 30 % strain. It allows bulk information on the developing glide polygonization to be obtained at the sample scale.

Our topographs show that the dislocation substructure becomes more and more heterogeneous with increasing temperature. A transition occurs at about 200 K. Below this temperature, there is no more visible lattice misorientation : primary and conjugate slip systems are nearly independent. The crystal plasticity is controlled only by the lattice friction.

Above 200 K, in addition to (111) walls, dislocation sheets are left along the two slip planes. It is believed that these sheets result from local interactions with the (101) $[\bar{1}11]$ conjugate system in order to relax primary screw stresses.

The existence of such sheets leads to a perceptible variation of the primary glissible screws density $\rho_m(\tau)$ with flow stress. This dependence modifies the macroscopic deformation parameters, even if, on the other hand, the elastic limit is still controlled by the lattice friction and much dependent on temperature. Up to 20 % strain there is observed :

— a slight but non-vanishing work-hardening rate, nearly constant in the range studied (about 10^{-3} μ),

— an *apparent* activation volume larger than the true one. It is no more a unique function of stress but depends on strain rate and on the nature of the deformation test. It decreases with strain as does $\partial \ln \rho_m / \partial \tau$.

At a given temperature the activation energy is nearly constant for any strain level ; furthermore it levels off with temperature to about 0.8 eV.

The origin of sheets is thought to be the attraction of primary and conjugate dislocations following the reaction :

$$\tfrac{1}{2}[111] + \tfrac{1}{2}[1\bar{1}\bar{1}] = [100]\,.$$

But relaxing internal stresses through this reaction needs building up [111] and [100] dislocations parallel to $[\bar{1}11]$ into a $[\bar{1}11]$ tilt sub-boundary (multipole), with one [100] for two [111], the boundary plane being (211). This in turn requires long enough primary and conjugate screw segments to bow out in the common cross-slip plane. This prominent cross-slip is possible only if the lattice friction is smaller than the acting internal stress aided by applied stresses, i. e., at high enough temperatures. Whether the actual structure of $(\bar{1}01)$ and (101) sheets can be locally viewed as made of parts of forming crude (211) multipoles cannot yet be firmly established without confirmation by electron microscopy, which is now planned in the laboratory.

Whatever the case, the existence of an average sheet plane $(\bar{1}01)$ or (101) with a $[1\bar{1}\ h]$ lattice rotation means that some torsion and probably some long range stresses are induced by these dislocation sheets, as also mentioned by Ströhle *et al.* [6].

On the other hand it is of interest to know what influence the orientation exerts upon the substructure rearrangement. So we plan also to investigate the plastic behaviour on the $(\bar{2}11)$ [111] slip system.

Acknowledgments. — The authors thank IRSID which supplied them with the as-grown α-iron single crystals and Dr. J. De Fouquet who measured the impurity content of the samples by Snoek internal friction analyses. This work received financial support from D. G. R. S. T. contract n° 71-7-2785.

References

[1] LUFT, A., RICHTER, J., REITZENSTEIN, W. and FINKE, P., Third Intern. Symp. *Reinstoffe in Wissenschaft und Technik* (Akademie-Verlag, Berlin) 1972, p. 285.

[2] LUFT, A. and KAUN, K., *Phys. Stat. Sol.* **37** (1970) 781.

[3] KUBIN, L. P., Thèse d'Etat (Université de Paris Sud, Centre d'Orsay), 1971, p. 106.

[4] BOWEN, D. K., CHRISTIAN, J. W. and TAYLOR, G., *Can. J. Phys.* **45** (1967) 903.

[5] SPITZIG, W. A. and KEH, A. S., *Acta Met.* **18** (1970) 611 and 1021.

[6] STRÖHLE, D., SESTAK, B. and WILKENS, M., *Z. Metallk.* **61** (1970) 642.

[7] KEH, A. S., SPITZIG, W. A. and NAKADA, Y., *Phil. Mag.* **23** (1971) 829.

[8] NEWKIRK, J. B., *Trans. A. I. M. E.* **215** (1959) 483.

[9] WILKENS, M., *Can. J. Phys.* **45** (1967) 567.

[10] FOXALL, R. A., DUESBERY, M. S. and HIRSCH, P. B., *Can. J. Phys.* **45** (1967) 607.

[11] AMELINCKX, S. and DEKEYSER, W., *Solid State Physics* (Academic Press, New York and London) vol. 8, 1959, p. 325.

[12] HAZZLEDINE, P. M., *J. Physique* **27** (1966) C3-210.

[13] FRIEDEL, J., *Dislocations* (International Series of monographs in Solid state physics, Pergamon, Gauthier-Villars) vol. 3, 1964, p. 250.

[14] LUFT, A., *Phys. Stat. Sol.* **42** (1970) 429.

[15] JAOUL, B., *Etude de la plasticité et application aux métaux* (Dunod, Paris) 1965, p. 191.

[16] GUIU, F. and PRATT, P. L., *Phys. Stat. Sol.* **6** (1964) 111.

[17] GROH, P. and CONTE, R., *Acta Met.* **19** (1971) 985.

[18] COULON, G., LECOQ, J. and ESCAIG, B., Compte Rendu de fin de contrat D. G. R. S. T.; n° 71, 7, 2785, 1972, p. 29.

[19] TAYLOR, G., CHRISTIAN, J. W., *Phil. Mag.* **15** (1967) 893.